JOURNAL OF MATERIALS SCIENCE **35** (2000) 3837–3848

The directional solidification of Pb-Sn alloys

E. ÇADIRLI
Niğde University, Faculty of Arts and Sciences, Department of Physics, Niğde-Turkey
M. GÜNDÜZ*
Erciyes University, Faculty of Arts and Sciences, Department of Physics, Kayseri-Turkey

Directional solidification experiments have been carried out on different Pb-Sn alloys as a function of temperature gradient G, growth rate V and cooling rate GV. The specimens were solidified under steady state condition with a constant temperature gradient (50 °C/cm) at a wide range of growth rates ((10–400) $\times 10^{-4}$ cm/s) and with a constant growth rate (17×10^{-4} cm/s) at a wide range of temperature gradient (10–55 °C/cm). The primary dendrite arm spacing, λ_1, and secondary dendrite arm spacing, λ_2, were evaluated. This structure parameters were expressed as functions of G, V and GV by using the linear regression analysis. The results were in good agreement with the previous works.

1. Introduction

Dendritic structures are very frequently observed during the solidification of alloys. The presence of dendritic structures during solidification with concomitant microsegregations is of interest since these solidification features are commonly found in many engineering materials and furthermore, greatly influence the mechanical behavior [1]. Many studies have been made of the "as-solidified" microstructures of binary alloys in order to determine experimentally the interdependence structure parameters, primary dendrite arm spacing (λ_1), secondary dendrite arm spacing (λ_2), and solidification parameters, temperature gradient (G), growth rate (V) and cooling rate (GV). In directional solidification experiments both the growth velocity, V, and the temperature gradient in the liquid, G, may be independently controlled, so that one may study the dependence of structure parameters (λ_1, λ_2), on either G (at constant V) or V (at constant G). Most of the studies [2–7] have shown that the primary dendrite arm spacing and secondary dendrite arm spacing decreases as the growth rate, temperature gradients and cooling rate are increased. In the last four decade there have been several studies of steady state directionally solidification applied to dendritic growth in alloy systems. These observations have led to the establishment of relationships of the following general type

$$(\lambda_1, \lambda_2) = k(G, V, GV)^{-n} \tag{1}$$

where k is a constant. These structure parameters (λ_1, λ_2) control the mechanical properties of the solidified alloys [8]. In the present work, directional solidification experiments have been carried out to obtain data on dendritic growth under constant growth rate, for different temperature gradients and constant temperature gradient, for different growth rates, in Pb-Sn alloys. In order to obtain relationships between structure parameters (λ_1, λ_2) and solidification parameters (G, V and GV) for each Pb-Sn alloy and each evaluated temperature gradient and growth rate, the primary dendrite arm spacings and secondary dendrite arm spacings were measured and also linear regression analysis were carried out for λ_1, λ_2. The results are compared with the previous works.

2. Experimental procedure

Pb-Sn alloys (Pb- 5, 10, 20, 35, 50, 95 wt.% Sn), were prepared by melting weighed quantities of Pb and Sn of high purity elements (99.99%) in a graphite crucible inserted in the vacuum melting furnace [9]. After allowing time for melt homogenisation, molten alloy was pored into the prepared graphite crucibles (250 mm in length 4 mm ID and 6.35 mm OD) in hot filling furnace [9]. Then each specimen was positioned in the Bridgman type furnace [10]. After holding to stabilize the thermal conditions, the specimen was grown under argon atmosphere by moving downwards at various constant rates by means of different speed synchronous motors. Specimens were solidified under steady state conditions with a constant growth velocity (approximately 17 μm/s) and different temperature gradients (10–55 °C/cm), with a constant temperature gradient (approximately 50 °C/cm), and different growth rates (10–400 μm/s). After steady state growth of 10–12 centimeters the samples were quenched by lowering them rapidly into the water reservoir. Also in order to find out the composition effect on structure parameters, directional solidification experiments were repeated for

* Author to whom all correspondence should be addressed.

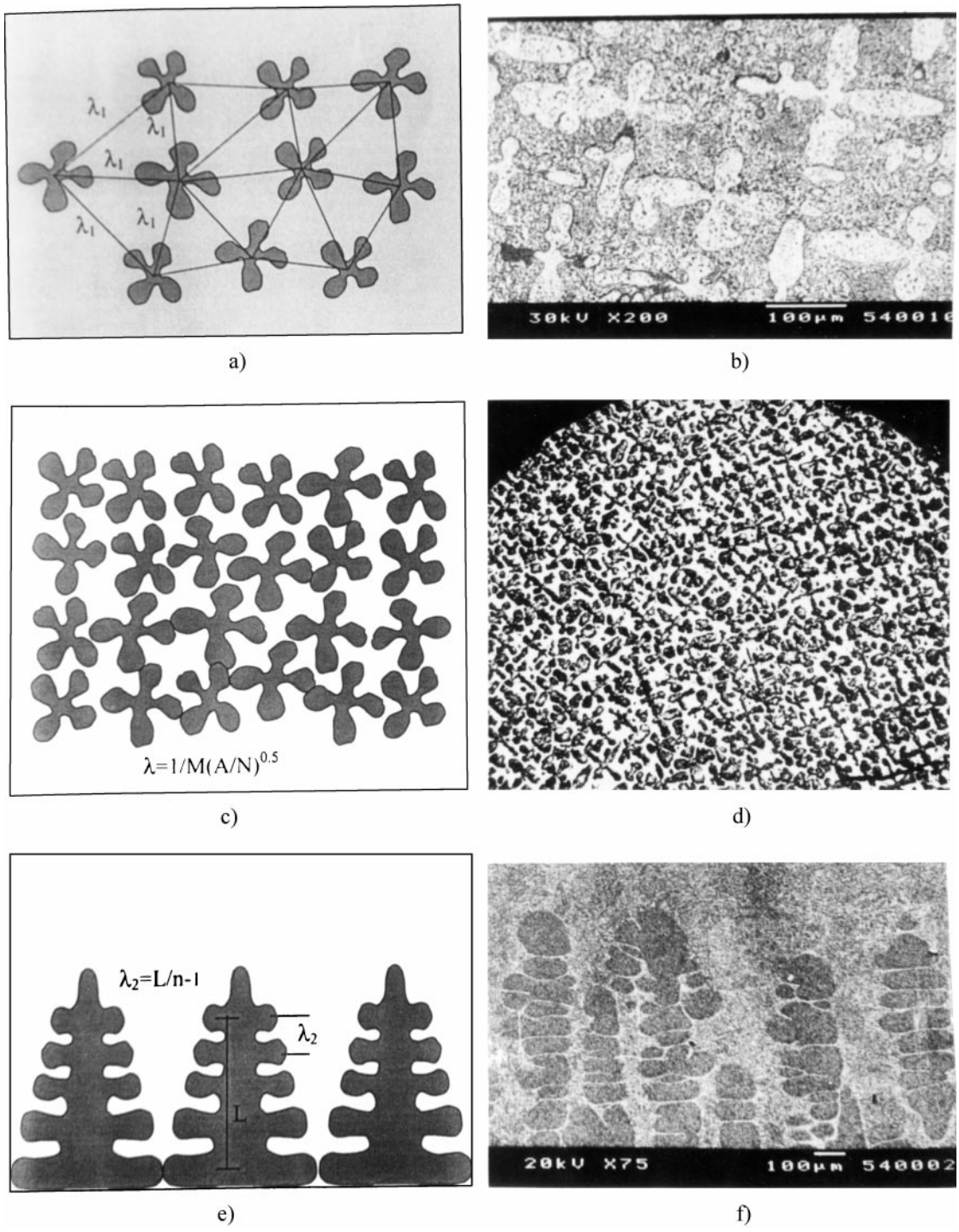

Figure 1 Definition of microstructure parameters (a, b) Schematic and photographic (SEM) illustration of primary dendrite arm spacing for Triangle Method (c, d) Schematic and photographic (OM) illustration of primary dendrite arm spacing for Area Counter Method (*M*: magnification factor, *A*: total area, *N*: number of primary dendrites) (e, f) Schematic and photographic (SEM) illustration of secondary dendrite arm spacing for Intercept Method (*L*: length, *n*: number of secondary arms).

six different Pb-Sn alloys (with different mushy zone depth) which cover the Sn rich side of the Pb-Sn phase diagrammes.

2.1. The measurement of temperature gradient and growth rates

The temperature of Bridgman type furnace was controlled by Pt/Pt-%13 Rd thermocouple placed between the heating element and the alumina tube. In the sample, temperature distribution was obtained by measuring the temperature during the heating and cooling by five chromel/alumel thermocouples (K-type) [11]. Accuracy of the thermocouples were checked by slowly solidifying the Pb-Sn samples (which where thermocouples placed parallel to the heat flow and perpendicular to the heat flow direction). The measured T difference was less than 0.5 °C with differently placed thermocouples. All through the experiment, the thermocouples were placed into the capillary alumina tubes (0.8 mm ID, 1.2 mm OD) which were positioned approximately 3 cm apart and parallel to the heat flow direction. All the thermocouple leads were taken to an ice/water cold junction, then to a WPA analog potentiometer and Kipp-Zonen recorder capable of recording

TABLE I The values of structure parameters (λ_1, λ_2) for different growth rates and temperature gradients for various compositions of Pb-Sn alloys in this work and other works

Composition (wt. %)	G (°C/cm)	V (cm/s) $\times 10^{-4}$	GV (°C/s)	λ_1 (cm)	λ_2 (cm)	Ref.
Pb-5 Sn	8.57–48.56	18.58	0.016–0.090	146.7–327.8	25.4–63.7	This work
	48.56	7.08–467.9	0.034–2.72	62.1–272.8	6.7–46.7	This work
Pb-10 Sn	14.49–55.55	16.36	0.027–0.090	143.1–262.4	20.2–53.7	This work
	55.55	8.89–417.2	0.049–2.31	40.7–193.7	5.5–34.4	This work
Pb-20 Sn	16.67–52.11	15.29	0.032–0.079	129.3–273.7	26.8–58.9	This work
	52.11	7.62–388.3	0.039–2.02	41.7–159.3	8.6–39.4	This work
Pb-35 Sn	17.11–49.50	18.45	0.030–0.091	130.6–182.3	13.8–29.9	This work
	49.50	7.23–357.3	0.035–1.77	59.9–164.6	5.3–26.2	This work
Pb-50 Sn	21.66–49.87	17.11	0.040–0.085	132.8–243.0	14.7–30.3	This work
	49.87	7.89–438.5	0.039–2.18	57.4–194.8	6.2–25.9	This work
Pb-95 Sn	16.45–55.01	18.75	0.031–0.103	114.6–262.0	24.7–57.1	This work
	55.01	8.12–446.1	0.045–2.45	49.9–251.3	8.5–69.1	This work
Pb-33.4 Sn	75	8	0.06	166	-	[2]
Pb-34 Sn	17	30	0.051	172	-	[2]
Pb-23.7 Sn	81	24	0.19	164	-	[2]
Pb-23.4 Sn	77	6	0.11	185	-	[2]
Pb-27 Sn	59	64	0.38	155	-	[2]
Pb-30.3 Sn	20	6	0.012	208	-	[2]
Pb-27.1 Sn	17	1	0.0017	240	-	[2]
Pb-10 Sn	110	10	0.11	115	-	[3]
Pb-16.5 Sn	101	6	0.06	172	-	[3]
Pb-23.2 Sn	77	4	0.03	185	-	[3]
Pb-54.7 Sn	105	10	0.10	234	-	[3]
Pb-57.9 Sn	67	40	0.27	177	-	[3]
Pb-10 Sn	72–545	9.96–207.1	0.071–11.28	73.5–162.5	-	[4]
Pb-20 Sn	49–369	1.67–207	0.008–7.63	80.8–163.9	-	[4]
Pb-40 Sn	18–356	0.38–408.2	0.0007–14.53	35–245	-	[4]
Pb-10 Sn	110	4.5–20	0.05–0.22	115–130	-	[5]
Pb-10 Sn	365–392	9.96–204	0.36–8.00	32.1–77.6	-	[6]
Pb-20 Sn	352–380	10.1–205.3	0.36–745	38.3–87	-	[6]
Pb-30 Sn	30.1–372	9.96–204	0.060–7.58	39.7–183.3	-	[6]
Pb-40 Sn	25.8–390	1.02–409	0.052–15.95	31.3–215.5	-	[6]
Pb-50 Sn	11–355	9.96–202.8	0.022–6.42	45.2–263.1	-	[6]

to 1 μV. The position of the thermocouples were measured after the quench and temperature of the thermocouples were recorded during the run, and when the second thermocouple at the solid-liquid interface, temperature of the second and third thermocouples were recorded simultaneously for measurement of G to obtain the temperature gradients on the solid/liquid interface. V and G can be controlled independently. Cooling water (with the constant temperature) level was always at the same position and the furnace temperature i.e the sample temperature was constant so the G. G can be changed by changing the sample temperature and the distance between the cooling water level and the hot stage. G can be kept constant because during the run, temperature of the cooler and heater part of the furnace was constant. The sample was pulled down to the water cooling tank with constant speed with the synchronized motors. It was found that the pulling speed was similar to the growth rate, that may be because of the metal sample holder and the graphite crucible which has good thermal conductivity. The growth rate was calculated with two different methods. In the first method, the values for the growth rate were calculated from the measurements of the time taken for the solid/liquid interface to pass the thermocouples separated by a known distance. In the second method, solidification time and solidification distance (on the longitudinal section of the polished sample) were measured. The ratio of the distances to the times were measured to obtain the growth rates and for both methods the growth rates were similar.

2.2. Metallographic examination

The unidirectionally grown quenched specimen were removed from the graphite crucibles, then ground to observe the solid-liquid interface and longitudinal section which included the quenched interface was separated from the specimen. This part was ground, polished to reveal the quenched interface. Furthermore the longitudinal and transverse sections of the grinded specimen was cold-mounted with epox-resin. The microstructure of the specimen was determined by metallographic analysis. Mechanical and electropolishing techniques were used to prepare transverse and longitudinal sections for both optical microscopy (OM) and scanning electron microscopy (SEM).

2.3. Measurement of primary dendrite arm spacings

As can be seen in Fig. 1, the primary dendrite arm spacings measured on the transverse section gave more accurate results than the primary dendrite arm spacings

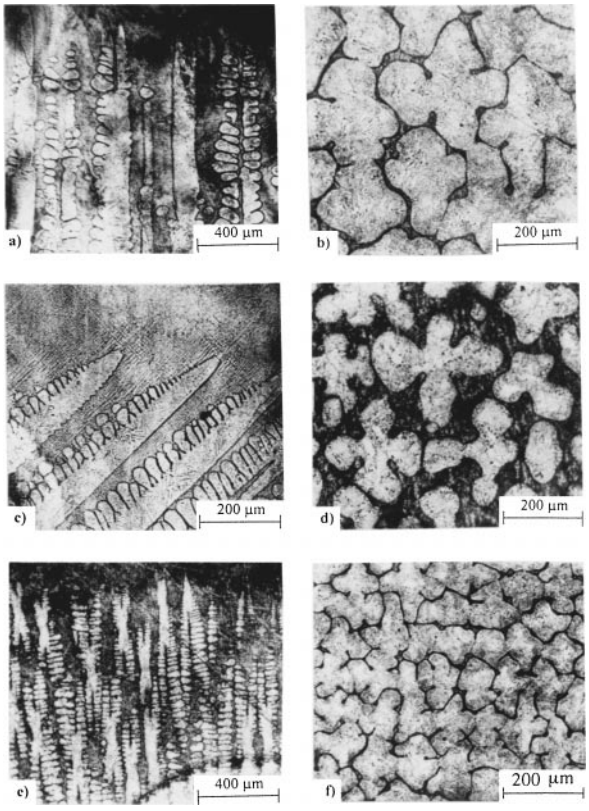

Figure 2 Dendritic structures of directionally solidified Pb-5wt.%Sn alloy for different growth rates and temperature gradients (a) Longitudinal section (b) Transverse section (G: 18.67 °C/cm, V: 18.58×10^{-4} cm/s) (c) Longitudinal section (d) Transverse section (G: 48.56 °C/cm, V: 7.08×10^{-4} cm/s) (e) Longitudinal section (f) Transverse section (G: 48.56 °C/cm, V: 81.02×10^{-4} cm/s).

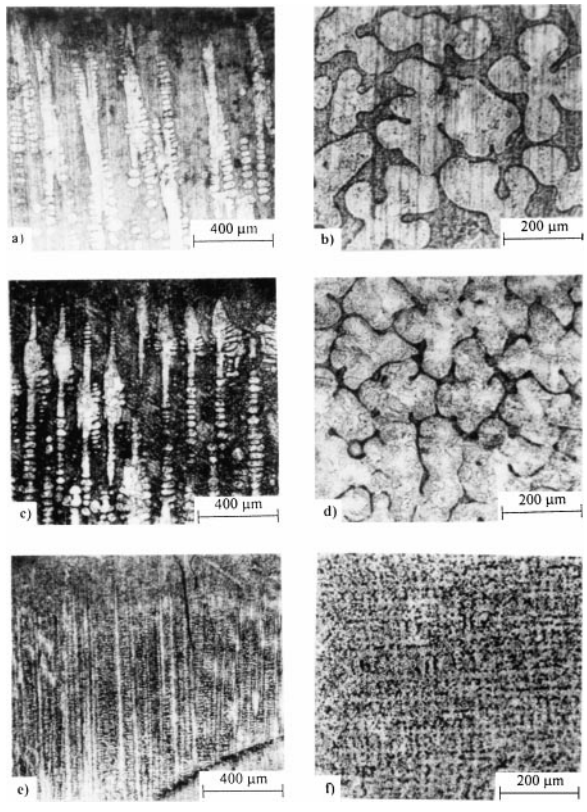

Figure 3 Dendritic structures of directionally solidified Pb-10wt.%Sn alloy for different growth rates and temperature gradients (a) Longitudinal section (b) Transverse section (G: 23.20 °C/cm, V: 16.36×10^{-4} cm/s) (c) Longitudinal section (d) Transverse section (G: 44.37 °C/cm, V: 16.36×10^{-4} cm/s) (e) Longitudinal section (f) Transverse section (G: 55.55 °C/cm, V: 417.24×10^{-4} cm/s).

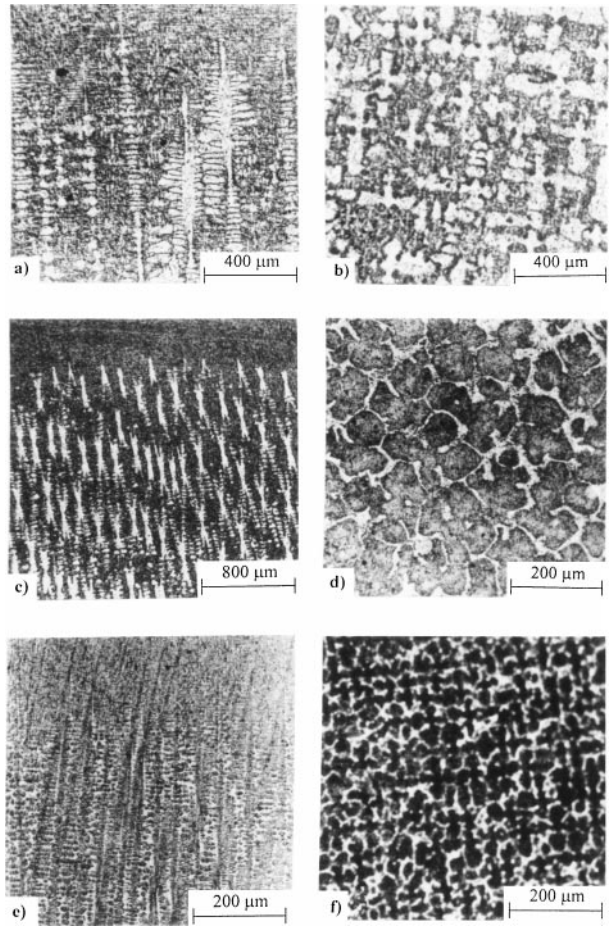

Figure 4 Dendritic structures of directionally solidified Pb-20wt.%Sn alloy for different growth rates and temperature gradients (a) Longitudinal section (b) Transverse section (G: 16.37 °C/cm, V: 15.29×10^{-4} cm/s) (c) Longitudinal section (d) Transverse section (G: 52.11 °C/cm, V: 15.29×10^{-4} cm/s) (e) Longitudinal section (f) Transverse section (G:52.11 °C/cm, V: 388.39×10^{-4} cm/s).

measured on the longitudinal section. There might be two reasons for this, firstly, λ_1 depends on the polished plane; secondly at least five times more primary dendrite arm spacing can be measured from the transverse section than the longitudinal section, this might give more accurately results. The measurements of λ_1 were carried on the transverse section rather than on the longitudinal section because of these reasons. Two different method were used for measurement of the primary dendrite arm spacings on transverse sections (Fig. 1a–d). The first method is the area counting method [12]. In this method, primary dendrite arm spacings were measured on the crossection (perpendicular to the growth direction) at least four different region for the each specimen. λ_1 is equal to $(1/M)\ (A/N)^{0.5}$ where M is the magnification factor, A is the total specimen crossection area (transverse section) and N is the number of primary dendrites on the crossection [12]. Depending on the growth conditions, 50–800 primary dendrite arm spacings were observed and counted on the corresponding specimen crossections. The second method is the triangle method [13]. The triangle occurred by joining the three neighbour dendrite centers and sides of the triangle are corresponded to λ_1. In this method at least 50–200 primary dendrite spacing were measured for the each specimen.

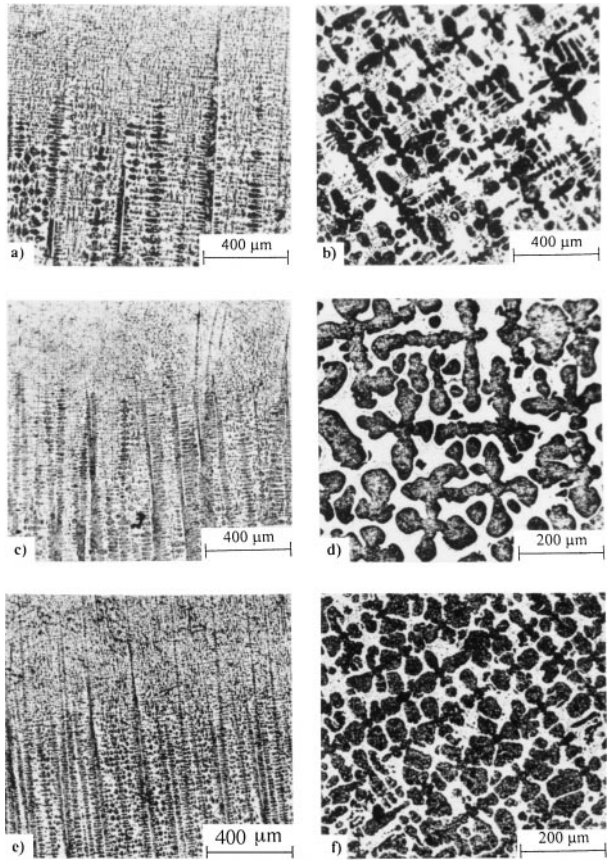

Figure 5 Dendritic structures of directionally solidified Pb-35wt.%Sn alloy for different growth rates and temperature gradients (a) Longitudinal section (b) Transverse section (G: 17.11 °C/cm, V: 18.45×10^{-4} cm/s) (c) Longitudinal section (d) Transverse section (G: 49.50 °C/cm, V: 18.45×10^{-4} cm/s) (e) Longitudinal section (f) Transverse section (G: 49.50 °C/cm, V: 76.76×10^{-4} cm/s).

2.4. Measurement of secondary dendrite arm spacings

Secondary dendrite arm spacings were measured by averaging the distance between adjacent side branches on the longitudinal section (parallel to growth direction) of a primary dendrite as function of distance from dendrite tip as can be seen in Fig. 1e and f. Each of the side branch spacing data reported here is the average of secondary dendrite arm spacings from 30–40 primary dendrites for each of the specimen.

3. Result and discussion

The measured primary dendrite arm spacings and secondary dendrite arm spacings for each composition and the previous results were given in Table I. In particularly λ_1 values were obtained in this work are in good agreement with λ_1 values which were obtained by other workers [2–6] on various compositions at the similar G, V, and GV values. The photographs of structures for unidirectionally solidified samples are given in Figs 2–7. The relationship between solidification parameters and structure parameters are shown in Figs 8–13. The mathematical relationships between solidification parameters and structure parameters were obtained by linear regression analysis for each composition and given in Table II. Primary dendrite arm spacings changed inversely proportionally to the temperature gradient,

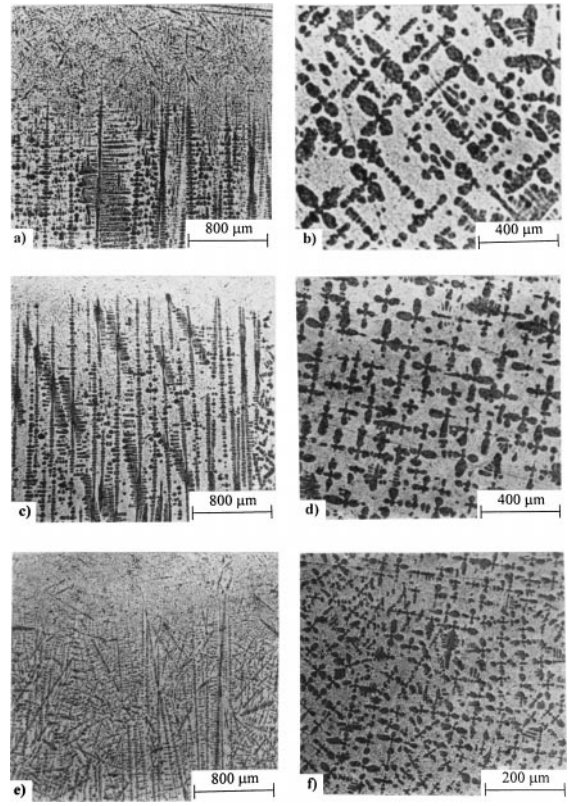

Figure 6 Dendritic structures of alloy directionally solidified Pb-50wt.%Sn for different growth rates and temperature gradients (a) Longitudinal section (b) Transverse section (G: 21.66 °C/cm, V: 17.11×10^{-4} cm/s) (c) Longitudinal section (d) Transverse section (G: 44.74 °C/cm, V: 17.11×10^{-4} cm/s) (e) Longitudinal section (f) Transverse section (G: 49.87 °C/cm, V: 119.23×10^{-4} cm/s).

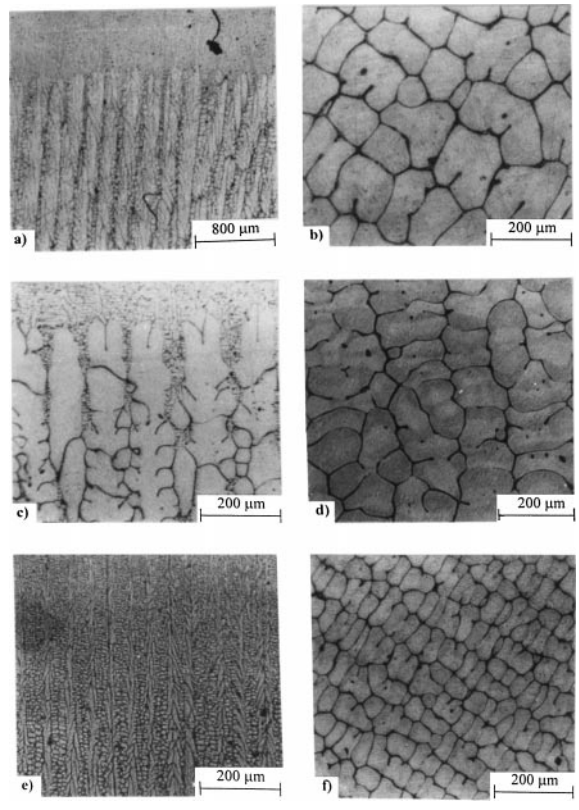

Figure 7 Dendritic structures of alloy directionally solidified Pb-95wt.%Sn for different growth rates and temperature gradients (a) Longitudinal section (b) Transverse section (G: 29.08 °C/cm, V: 18.75×10^{-4} cm/s) (c) Longitudinal section (d) Transverse section (G: 55.01 °C/cm, V: 18.75×10^{-4} cm/s) (e) Longitudinal section (f) Transverse section (G: 55.01 °C/cm, V: 153.06×10^{-4} cm/s).

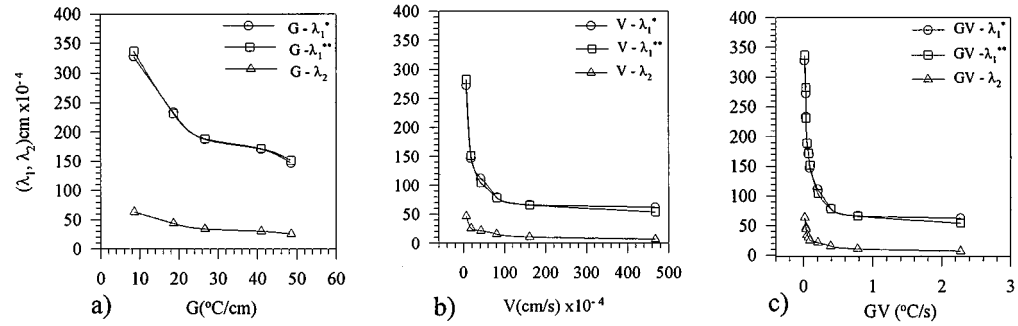

Figure 8 The plot of λ_1, λ_2 versus temperature gradient G, growth rate V, and cooling rate GV for Pb-5wt.%Sn alloy (a) The plot of λ_1, λ_2 versus G (b) The plot of λ_1, λ_2 versus V (c) The plot of λ_1, λ_2 versus GV.

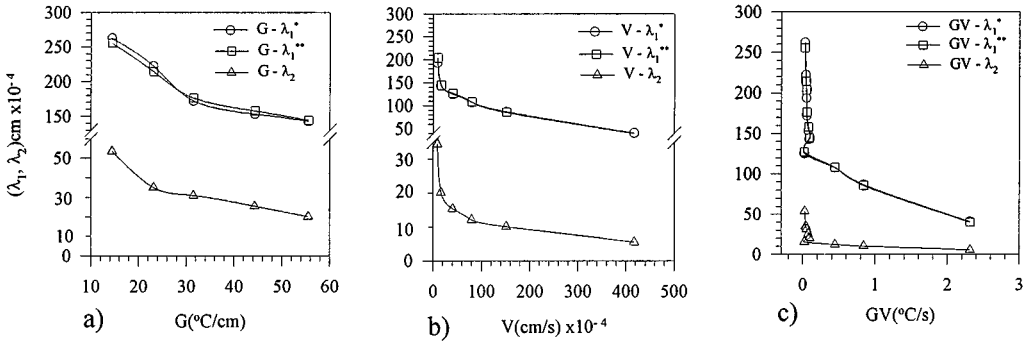

Figure 9 The plot of λ_1, λ_2 versus temperature gradient G, growth rate V, and cooling rate GV for Pb-10wt.%Sn alloy (a) The plot of λ_1, λ_2 versus G (b) The plot of λ_1, λ_2 versus V (c) The plot of λ_1, λ_2 versus GV.

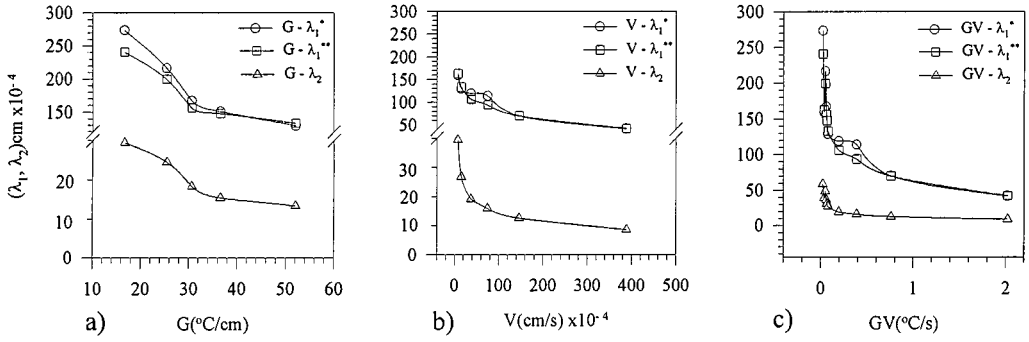

Figure 10 The plot of λ_1, λ_2 versus temperature gradient G, growth rate V, and cooling rate GV for Pb-20wt.%Sn alloy (a) The plot of λ_1, λ_2 versus G (b) The plot of λ_1, λ_2 versus V (c) The plot of λ_1, λ_2 versus GV.

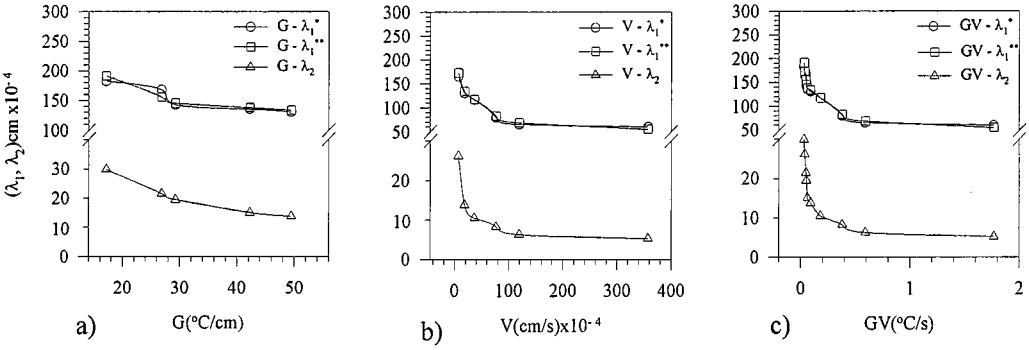

Figure 11 The plot of λ_1, λ_2 versus temperature gradient G, growth rate V, and cooling rate GV for Pb-35wt.%Sn alloy (a) The plot of λ_1, λ_2 versus G (b) The plot of λ_1, λ_2 versus V (c) The plot of λ_1, λ_2 versus GV.

growth rate and cooling rate. The exponent value for λ_1 changed for each of the solidification parameters (G, V, GV), 0.32–0.71, 0.29–0.40, and 0.29–0.40 range respectively. The exponent values are similar in the relationships among λ_1 and G and V in Pb-5wt.%Sn, Pb-10wt.%Sn, and Pb-35wt.%Sn alloys. The dependent of λ_1 to relate G is approximately twice higher than V. The primary dendrite arm spacings were in good agreement with the values obtained by Klaren *et al.* for similar GV values at the same composition

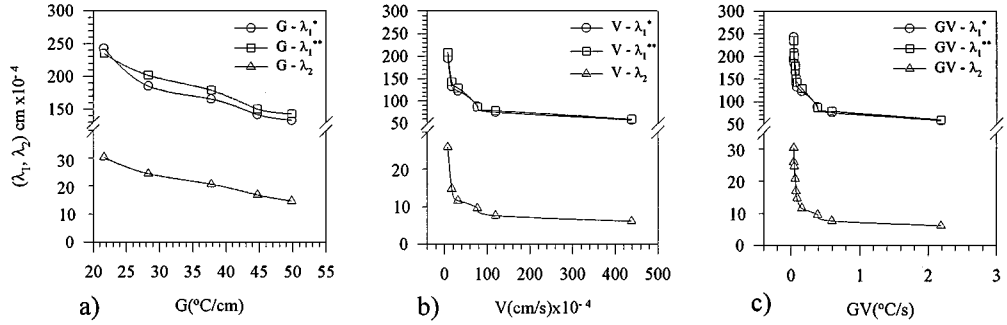

Figure 12 The plot of λ_1, λ_2 versus temperature gradient G, growth rate V, and cooling rate GV for Pb-50wt.%Sn alloy (a) The plot of λ_1, λ_2 versus G (b) The plot of λ_1, λ_2 versus V (c) The plot of λ_1, λ_2 versus GV.

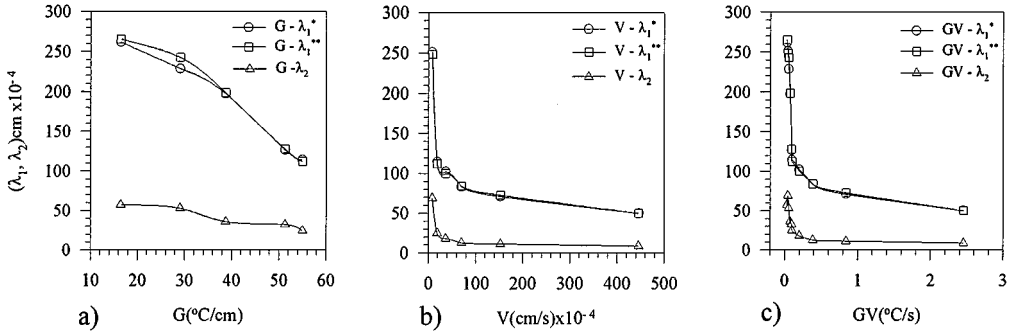

Figure 13 The plot of λ_1, λ_2 versus temperature gradient G, growth rate V, and cooling rate GV for Pb-95wt.%Sn alloy (a) The plot of λ_1, λ_2 versus G (b) The plot of λ_1, λ_2 versus V (c) The plot of λ_1, λ_2 versus GV.

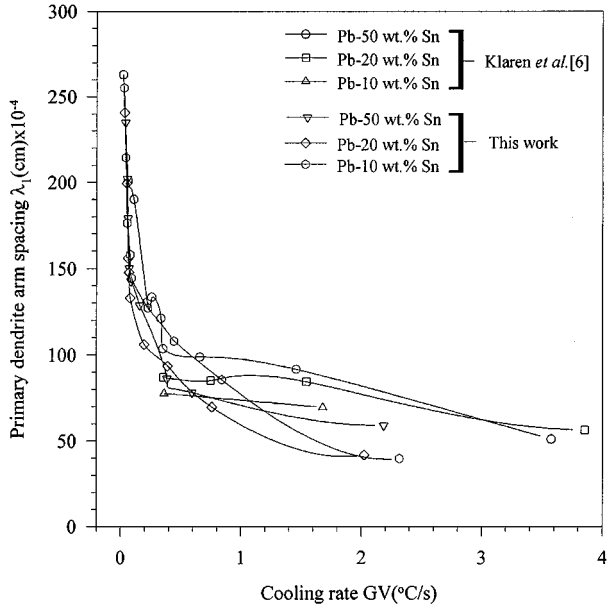

Figure 14 The plot of λ_1 versus cooling rate, GV for different composition in the Pb-Sn alloys.

Pb-Sn alloys as can be seen in Fig. 14. The comparison of experimentally obtained primary dendrite arm spacings with the calculated primary dendrite arm spacings by Hunt model [14] and Kurz-Fisher model [15] are given in Fig. 15 (physical parameters of Pb-Sn alloys used in λ_1 calculations for Kurz-Fisher and Hunt models are given in Appendix). The experimental results were in good agreement with the results calculated by Hunt model, but the results calculated by Kurz-Fisher model for all compositions were too large from our experimental results. The experimental primary dendrite arm spacings were in good agreement with the primary dendrite arm spacings calculated by Hunt model in all growth rates for Pb-5wt.%Sn, Pb-10wt.%Sn and Pb-20wt.Sn alloys. The experimental primary dendrite arm spacings were in fairly good agreement with primary dendrite arm spacings calculated by Hunt model in low growth rates for Pb-35wt.%Sn, Pb-50wt.%Sn and Pb-95wt.Sn alloys. However, it was found that the difference increases between experimental primary dendrite arm spacings and the primary dendrite arm spacings calculated by Hunt model for the higher growth rates Fig. 15. The similar results were found by other workers [16–20].

The relationships between the results which were obtained in this work and by previous workers for similar composition alloys are given in Table III. The relationships which were obtained between λ_1 and V for Pb-5wt.%Sn, Pb-10wt.%Sn and Pb-95wt.%Sn compositions in this work aligns with the relationships obtained by Mason *et al.* [4], with similar G, V, and GV for Pb-10wt.%Sn alloy. Besides, relationships which were obtained between λ_1 and G in this work for Pb-5, 10 and 35wt.%Sn alloys are in good agreement with relationship obtained by Klaren *et al.* [6] with near GV values.

Secondary dendrite arm spacing changed inversely proportional to temperature gradient, growth rate and cooling rate. The exponent values for λ_2 changed for each solidification parameter (G, V, GV), 0.50–0.82, 0.34–0.49, and 0.38–0.51 range respectively. The dependence of λ_2 to relate G and V approximately the same for Pb-5wt.%Sn alloy and the other alloys Pb-10wt.%Sn, Pb-95wt.%Sn and Pb-50wt.%Sn alloys. On the other hand, dependence of λ_2 to relate G is

TABLE II The relationships between structure parameters and solidification parameters for various compositions of Pb-Sn alloys

Composition: Pb-5wt.%Sn		
$\lambda_1^* = k_1 G^{-0.45}$	$k_1 = 8.73 \times 10^{-2}$ ($cm^{0.55}$ $°C^{0.45}$)	$r_1 = -0.995$
$\lambda_1^{**} = k_2 G^{-0.44}$	$k_2 = 8.68 \times 10^{-2}$ ($cm^{0.56}$ $°C^{0.44}$)	$r_2 = -0.997$
$\lambda_1^* = k_3 V^{-0.36}$	$k_3 = 1.67 \times 10^{-3}$ ($cm^{1.36}$ $s^{-0.36}$)	$r_3 = -0.957$
$\lambda_1^{**} = k_4 V^{-0.40}$	$k_4 = 1.35 \times 10^{-3}$ ($cm^{1.40}$ $s^{-0.40}$)	$r_4 = -0.984$
$\lambda_1^* = k_5 (GV)^{-0.37}$	$k_5 = 6.65 \times 10^{-3}$ (cm $°C^{0.37}$ $s^{-0.37}$)	$r_5 = -0.997$
$\lambda_1^{**} = k_6 (GV)^{-0.40}$	$k_6 = 6.23 \times 10^{-3}$ (cm $°C^{0.40}$ $s^{-0.40}$)	$r_6 = -0.984$
$\lambda_2 = k_7 G^{-0.50}$	$k_7 = 1.83 \times 10^{-2}$ ($cm^{0.50}$ $°C^{0.50}$)	$r_7 = -0.990$
$\lambda_2 = k_8 V^{-0.45}$	$k_8 = 1.71 \times 10^{-4}$ ($cm^{1.45}$ $s^{-0.45}$)	$r_8 = -0.994$
$\lambda_2 = k_9 G V^{-0.45}$	$k_9 = 9.76 \times 10^{-4}$ (cm $°C^{0.45}$ $s^{-0.45}$)	$r_9 = -0.995$
Composition: Pb-10wt.%Sn		
$\lambda_1^* = k_{10} G^{-0.47}$	$k_{10} = 9.25 \times 10^{-2}$ ($cm^{0.53}$ $°C^{0.47}$)	$r_{10} = -0.985$
$\lambda_1^{**} = k_{11} G^{-0.43}$	$k_{11} = 8.12 \times 10^{-2}$ ($cm^{0.57}$ $°C^{0.43}$)	$r_{11} = -0.995$
$\lambda_1^* = k_{12} V^{-0.36}$	$k_{12} = 1.64 \times 10^{-3}$ ($cm^{1.36}$ $s^{-0.36}$)	$r_{12} = -0.953$
$\lambda_1^{**} = k_{13} V^{-0.38}$	$k_{13} = 1.51 \times 10^{-3}$ ($cm^{1.38}$ $s^{-0.38}$)	$r_{13} = -0.958$
$\lambda_1^* = k_{14} (GV)^{-0.35}$	$k_{14} = 6.90 \times 10^{-3}$ (cm $°C^{0.35}$ $s^{-0.35}$)	$r_{14} = -0.966$
$\lambda_1^{**} = k_{15} (GV)^{-0.36}$	$k_{15} = 6.82 \times 10^{-3}$ (cm $°C^{0.36}$ $s^{-0.36}$)	$r_{15} = -0.972$
$\lambda_2 = k_{16} G^{-0.68}$	$k_{16} = 3.21 \times 10^{-2}$ ($cm^{0.32}$ $°C^{0.68}$)	$r_{16} = -0.989$
$\lambda_2 = k_{17} V^{-0.43}$	$k_{17} = 1.49 \times 10^{-4}$ ($cm^{1.43}$ $s^{-0.43}$)	$r_{17} = -0.985$
$\lambda_2 = k_{18} (GV)^{-0.46}$	$k_{18} = 8.25 \times 10^{-4}$ (cm $°C^{0.46}$ $s^{-0.46}$)	$r_{18} = -0.986$
Composition: Pb-20wt.%Sn		
$\lambda_1^* = k_{19} G^{-0.69}$	$k_{19} = 1.92 \times 10^{-1}$ ($cm^{0.31}$ $°C^{0.69}$)	$r_{19} = -0.980$
$\lambda_1^{**} = k_{20} G^{-0.55}$	$k_{20} = 1.20 \times 10^{-1}$ ($cm^{0.45}$ $°C^{0.55}$)	$r_{20} = -0.964$
$\lambda_1^* = k_{21} V^{-0.32}$	$k_{21} = 1.84 \times 10^{-3}$ ($cm^{1.32}$ $s^{-0.32}$)	$r_{21} = -0.936$
$\lambda_1^{**} = k_{22} V^{-0.33}$	$k_{22} = 1.65 \times 10^{-3}$ ($cm^{1.33}$ $s^{-0.33}$)	$r_{22} = -0.982$
$\lambda_1^* = k_{23} (GV)^{-0.37}$	$k_{23} = 6.25 \times 10^{-3}$ (cm $°C^{0.37}$ $s^{-0.37}$)	$r_{23} = -0.947$
$\lambda_1^{**} = k_{24} (GV)^{-0.37}$	$k_{24} = 5.93 \times 10^{-3}$ (cm $°C^{0.37}$ $s^{-0.37}$)	$r_{24} = -0.977$
$\lambda_2 = k_{25} G^{-0.74}$	$k_{25} = 4.90 \times 10^{-2}$ ($cm^{0.26}$ $°C^{0.74}$)	$r_{25} = -0.975$
$\lambda_2 = k_{26} V^{-0.37}$	$k_{26} = 2.60 \times 10^{-4}$ ($cm^{1.37}$ $s^{-0.37)}$	$r_{26} = -0.995$
$\lambda_2 = k_{27} (GV)^{-0.43}$	$k_{27} = 1.09 \times 10^{-3}$ (cm $°C^{0.43}$ $s^{-0.43}$)	$r_{27} = -0.974$
Composition: Pb-35wt.%Sn		
$\lambda_1^* = k_{28} G^{-0.33}$	$k_{28} = 4.65 \times 10^{-2}$ ($cm^{0.67}$ $°C^{.33}$)	$r_{28} = -0.944$
$\lambda_1^{**} = k_{29} G^{-0.32}$	$k_{29} = 4.61 \times 10^{-2}$ ($cm^{0.68}$ $°C^{0.32}$)	$r_{29} = -0.960$
$\lambda_1^* = k_{30} V^{-0.29}$	$k_{30} = 2.14 \times 10^{-3}$ ($cm^{1.29}$ $s^{-0.29}$)	$r_{30} = -0.974$
$\lambda_1^{**} = k_{31} V^{-0.31}$	$k_{31} = 1.91 \times 10^{-3}$ ($cm^{1.31}$ $s^{-0.31}$)	$r_{31} = -0.989$
$\lambda_1^* = k_{32} (GV)^{-0.29}$	$k_{32} = 6.47 \times 10^{-3}$ (cm $°C^{0.29}$ $s^{-0.29}$)	$r_{32} = -0.980$
$\lambda_1^{**} = k_{33} (GV)^{-0.30}$	$k_{33} = 6.35 \times 10^{-3}$ (cm $°C^{0.30}$ $s^{-0.30}$)	$r_{33} = -0.990$
$\lambda_2 = k_{34} G^{-0.73}$	$k_{34} = 2.40 \times 10^{-2}$ ($cm^{0.27}$ $°C^{0.73}$)	$r_{34} = -0.998$
$\lambda_2 = k_{35} V^{-0.41}$	$k_{35} = 1.16 \times 10^{-4}$ ($cm^{1.41}$ $s^{-0.41}$)	$r_{35} = -0.974$
$\lambda_2 = k_{36} (GV)^{-0.43}$	$k_{36} = 5.61 \times 10^{-4}$ (cm $°C^{0.43}$ $s^{-0.43}$)	$r_{36} = -0.974$
Composition: Pb-50wt.%Sn		
$\lambda_1^* = k_{37} G^{-0.70}$	$k_{37} = 2.01 \times 10^{-1}$ ($cm^{0.30}$ $°C^{0.70}$)	$r_{37} = -0.995$
$\lambda_1^{**} = k_{38} G^{-0.60}$	$k_{38} = 1.49 \times 10^{-1}$ ($cm^{0.40}$ $°C^{0.60}$)	$r_{38} = -0.997$
$\lambda_1^* = k_{39} V^{-0.30}$	$k_{39} = 2.09 \times 10^{-3}$ ($cm^{1.70}$ $s^{-0.30}$)	$r_{39} = -0.957$
$\lambda_1^{**} = k_{40} V^{-0.31}$	$k_{40} = 2.04 \times 10^{-3}$ ($cm^{1.60}$ $s^{-0.60}$)	$r_{40} = -0.971$
$\lambda_1^* = k_{41} (GV)^{-0.33}$	$k_{41} = 6.70 \times 10^{-3}$ (cm $°C^{0.33}$ $s^{-0.33}$)	$r_{41} = -0.977$
$\lambda_1^{**} = k_{42} (GV)^{-0.34}$	$k_{42} = 6.88 \times 10^{-3}$ (cm $°C^{0.34}$ $s^{-0.34}$)	$r_{42} = -0.984$
$\lambda_2 = k_{43} G^{-0.82}$	$k_{43} = 3.52 \times 10^{-2}$ ($cm^{0.18}$ $°C^{0.82}$)	$r_{43} = -0.990$
$\lambda_2 = k_{44} V^{-0.34}$	$k_{44} = 1.88 \times 10^{-4}$ ($cm^{1.34}$ $s^{-0.34}$)	$r_{44} = -0.994$
$\lambda_2 = k_{45} (GV)^{-0.38}$	$k_{45} = 6.91 \times 10^{-4}$ (cm $°C^{0.438}$ $s^{-0.38}$)	$r_{45} = -0.995$
Composition: Pb-95wt.%Sn		
$\lambda_1^* = k_{46} G^{-0.69}$	$k_{46} = 2.03 \times 10^{-1}$ ($cm^{0.31}$ $°C^{0.69}$)	$r_{46} = -0.915$
$\lambda_1^{**} = k_{47} G^{-0.71}$	$k_{47} = 2.23 \times 10^{-1}$ ($cm^{0.29}$ $°C^{0.71}$)	$r_{47} = -0.904$
$\lambda_1^* = k_{48} V^{-0.36}$	$k_{48} = 1.50 \times 10^{-3}$ ($cm^{1.36}$ $s^{-0.36}$)	$r_{48} = -0.951$
$\lambda_1^{**} = k_{49} V^{-0.35}$	$k_{49} = 1.52 \times 10^{-3}$ ($cm^{1.35}$ $s^{-0.35}$)	$r_{49} = -0.945$
$\lambda_1^* = k_{50} (GV)^{-0.39}$	$k_{50} = 6.25 \times 10^{-3}$ (cm $°C^{0.39}$ $s^{-0.39}$)	$r_{50} = -0.956$
$\lambda_1^{**} = k_{51} (GV)^{-0.40}$	$k_{51} = 6.28 \times 10^{-3}$ (cm $°C^{0.40}$ $s^{-0.40}$)	$r_{51} = -0.949$
$\lambda_2 = k_{52} G^{-0.66}$	$k_{52} = 4.02 \times 10^{-2}$ ($cm^{0.34}$ $°C^{0.66}$)	$r_{52} = -0.918$
$\lambda_2 = k_{53} V^{-0.49}$	$k_{53} = 1.46 \times 10^{-4}$ ($cm^{1.49}$ $s^{-0.49}$)	$r_{53} = -0.930$
$\lambda_2 = k_{54} (GV)^{-0.51}$	$k_{54} = 1.02 \times 10^{-3}$ (cm $°C^{0.51}$ $s^{-0.51}$)	$r_{54} = -0.954$

*Triangle method, **Area counting method

twice higher than V in Pb-20wt.%Sn, Pb-35wt.%Sn and Pb-50wt.%Sn alloys. The exponent value is -0.82 in the relationship between λ_2 and G for Pb-50wt.%Sn alloy. This value is higher than the whole exponent values in the relationships obtained and λ_2 is more rapidly decreasing with term of G increasing. In relation to G and V values obtained for λ_1 and λ_2 in the Pb-20wt.%Sn alloy, it is possible to state that growth rate was higher than the values obtained for Pb-5wt.%Sn and Pb-10wt.%Sn alloys. The ratios of λ_1/λ_2 with term of cooling rate increase are given in Fig. 16. As can be seen from Fig. 16 the ratios of λ_1/λ_2 changed approximately 4–12 times, values range for various compositions. The ratios of λ_1/λ_2 tend to increase continuously

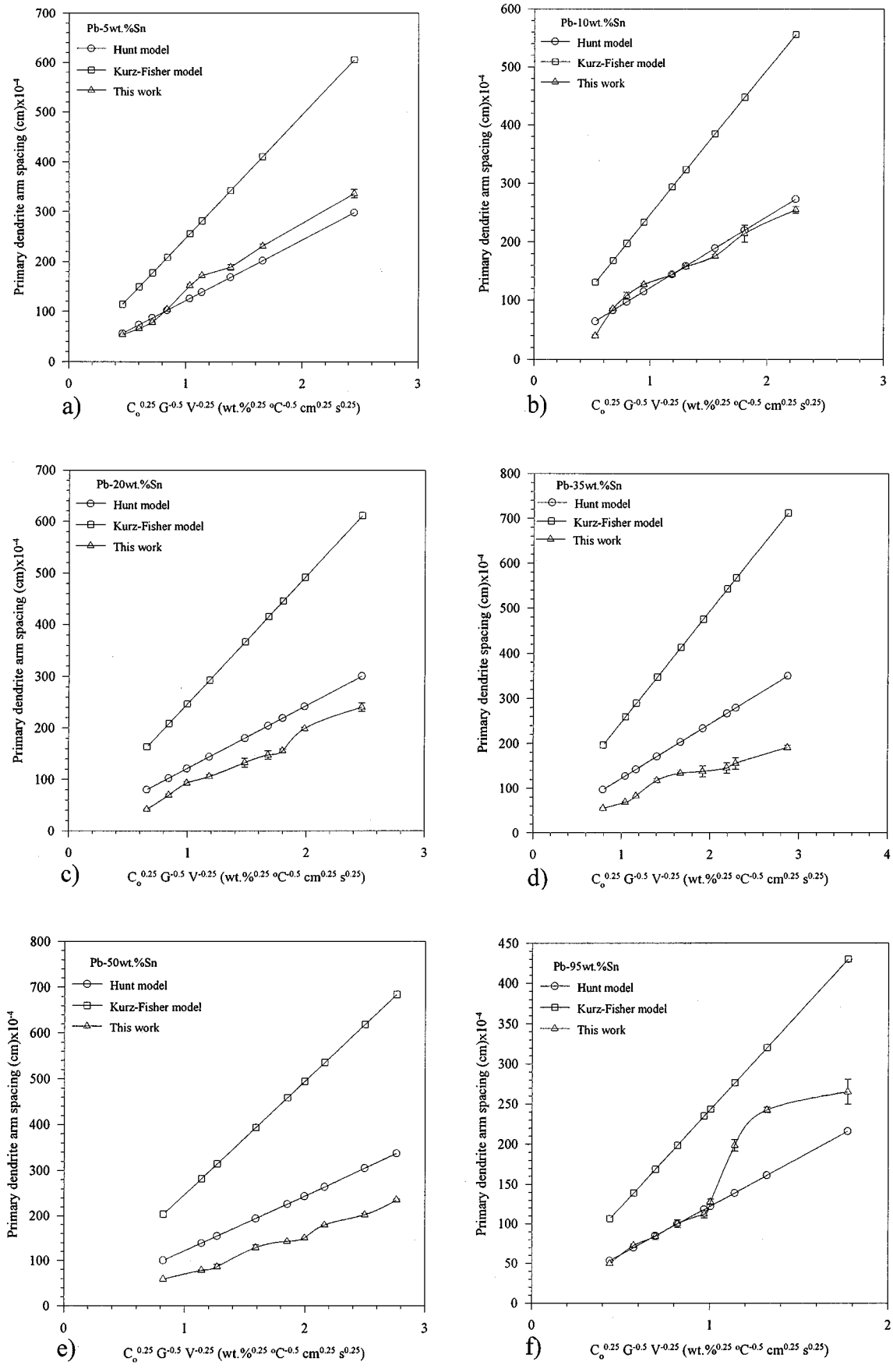

Figure 15 The comparison of the experimentally obtained λ_1 values with the λ_1 values obtained from Hunt model [14] and Kurz-Fisher model [15] for different Pb-Sn alloys (a) Pb-5wt.%Sn, (b) Pb-10wt.%Sn, (c) Pb-20wt.%Sn, (d) Pb-35wt.%Sn, (e) Pb-50wt.%Sn, (f) Pb-95wt.%Sn.

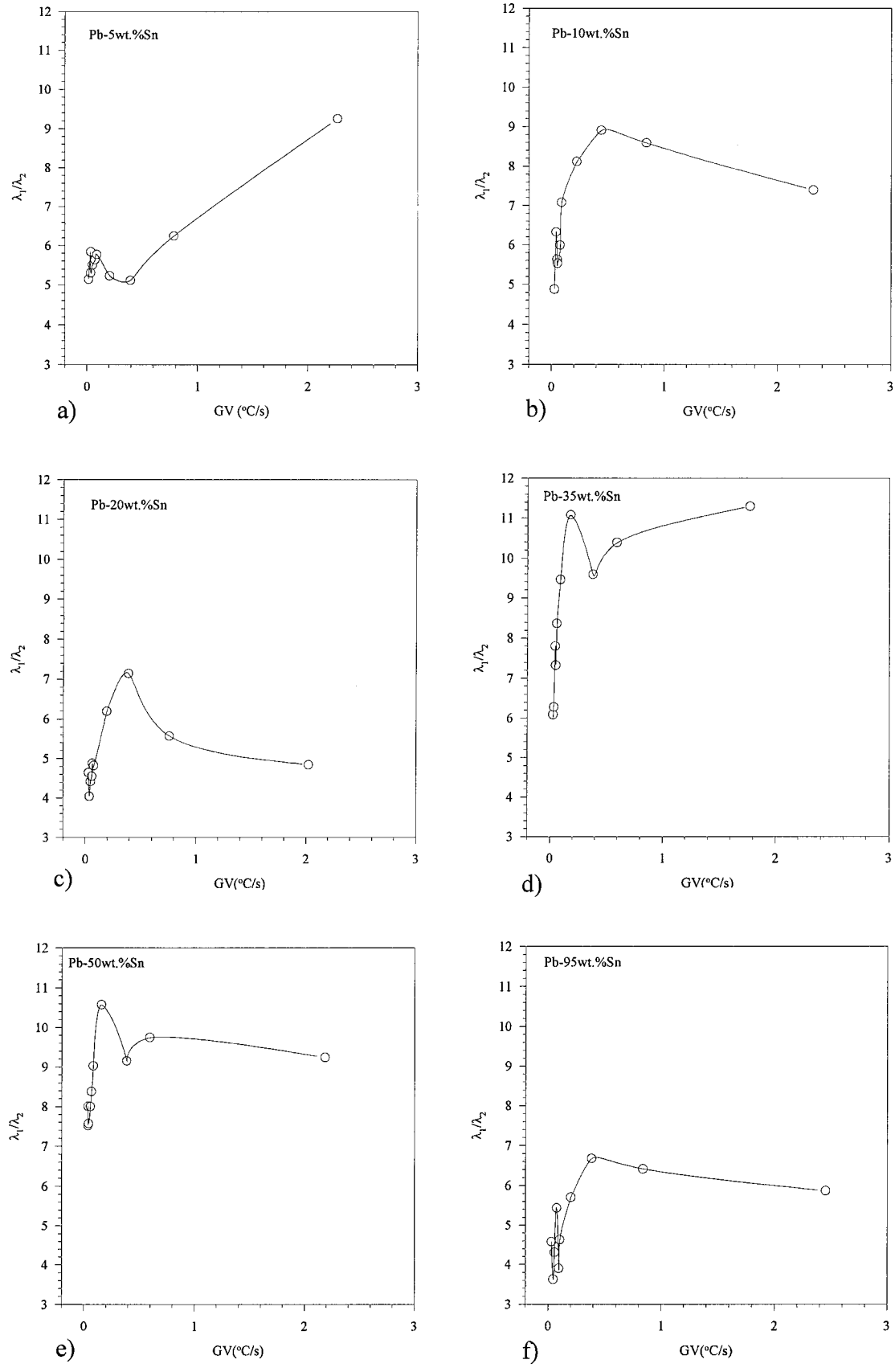

Figure 16 The plots of λ_1/λ_2 ratios versus cooling rates *GV*, for different compositions of Pb-Sn alloys.

for Pb-5wt.%Sn composition, but this increase carried on until approximately (0.3–0.4 °C/s) cooling rates for all other compositions. Also for other compositions, ratios take approximately a constant value following the evident cooling rate. As can be seen from the exponent value in Table III, both λ_1 and λ_2 were shown to decrease by approximately same degree, particularly for the composition values containing 10, 20 and 50 wt.%Sn. The dendritic structure of Pb-95wt.%Sn alloy is different than the other alloys, it presents a peeled

TABLE III Relationships between λ_1, λ_2 and G, V, and GV obtained for different compositions

Alloy	Composition (wt. %)	G (°C/cm)	V (cm/s) $\times 10^{-4}$	GV (°C/s)	Relationships	Ref.
Pb-Sn	10–57.9 Sn	59–110	4–66	0.023–0.73	$\lambda_1 = kG^{-0.5}\,V^{-0.25}\,C^{0.25}$	[3]
Pb-Sn	40 Sn	107	45–400	0.48–4.28	$\lambda_1 = kV^{-0.39}$	[4]
Pb-Sn	10–50 Sn	11–392	1.02–409	0.001–16.03	$\lambda_1 = k\,G^{-0.33}\,V^{-0.45}$	[6]
Pb-Sn	5 Sn	8.57–48.56	7.08–467.06	0.016–2.72	$\lambda_1 = k\,G^{-0.45}$	This work
					$\lambda_1 = k\,V^{-0.36}$	This work
					$\lambda_1 = k\,(GV)^{-0.37}$	This work
					$\lambda_2 = k\,G^{-0.50}$	This work
					$\lambda_2 = k\,V^{-0.45}$	This work
					$\lambda_2 = k\,(GV)^{-0.45}$	This work
Pb-Sn	10 Sn	14.49–55.55	8.89–417.24	0.027–2.31	$\lambda_1 = k\,G^{-0.47}$	This work
					$\lambda_1 = k\,V^{-0.36}$	This work
					$\lambda_1 = k\,(GV)^{-0.35}$	This work
					$\lambda_2 = k\,G^{-0.68}$	This work
					$\lambda_2 = k\,V^{-0.43}$	This work
					$\lambda_2 = k\,(GV)^{-0.36}$	This work
Pb-Sn	20 Sn	16.67–52.11	7.62–388.39	0.032–2.02	$\lambda_1 = k\,G^{-0.69}$	This work
					$\lambda_1 = k\,V^{-0.32}$	This work
					$\lambda_1 = k\,(GV)^{-0.37}$	This work
					$\lambda_2 = k\,G^{-0.74}$	This work
					$\lambda_2 = k\,V^{-0.37}$	This work
					$\lambda_2 = k\,(GV)^{-0.43}$	This work
Pb-Sn	35 Sn	17.11–49.50	7.23–357.38	0.030–1.76	$\lambda_1 = k\,G^{-0.33}$	This work
					$\lambda_1 = k\,V^{-0.29}$	This work
					$\lambda_1 = k\,(GV)^{-0.29}$	This work
					$\lambda_2 = k\,G^{-0.73}$	This work
					$\lambda_2 = k\,V^{-0.41}$	This work
					$\lambda_2 = k\,(GV)^{-0.43}$	This work
Pb-Sn	50 Sn	21.66–49.87	7.89–438.55	0.039–2.18	$\lambda_1 = k\,G^{-0.70}$	This work
					$\lambda_1 = k\,V^{-0.30}$	This work
					$\lambda_1 = k\,(GV)^{-0.33}$	This work
					$\lambda_2 = k\,G^{-0.82}$	This work
					$\lambda_2 = k\,V^{-0.34}$	This work
					$\lambda_2 = k\,(GV)^{-0.38}$	This work
Pb-Sn	95 Sn	16.45–55.01	8.12–446.16	0.030–2.45	$\lambda_1 = k\,G^{-0.69}$	This work
					$\lambda_1 = k\,V^{-0.36}$	This work
					$\lambda_1 = k\,(GV)^{-0.39}$	This work
					$\lambda_2 = k\,G^{-0.66}$	This work
					$\lambda_2 = k\,V^{-0.49}$	This work
					$\lambda_2 = k\,(GV)^{-0.51}$	This work

corn shape. The liquid phase between dendrites on the transverse section is to become small near to interface, in the photographs concerning Pb-95wt.%Sn composition alloy given in Fig. 7, the structure is like a zip fastener.

4. Conclusion

1. Under steady state conditions, primary dendrite arm spacings and secondary dendrite arm spacings were observed to decrease while the temperature gradient in the liquid the growth rate and cooling rate were observed to increase.

2. Secondary dendrite arm spacing was found to be more dependent on the temperature gradient, growth rate and cooling rate rather than primary dendrite arm spacing.

3. The dendritic structures become small in accordance with the increase in the solidification parameters.

4. The primary dendrite arm spacings were found in good agreement with the values given in Hunt model [14]; however, in Kurz-Fisher model [15] the experimental values presented are too large.

Change of the structure parameters affects the mechanical and the physical properties of the material [8, 21]. Owing to this directional solidification under evident solidification condition of materials, change of mechanical and physical properties of materials plays a very important role.

Appendix

Physical parameters of Pb-Sn alloys used in λ_1 calculations for Hunt [14] and Kurz-Fisher models [15]

$$\Gamma_\alpha = 7.9 \times 10^{-6}\,(\text{K cm}) \quad [22]$$

$$\Gamma_\beta = 4.8 \times 10^{-6}\,(\text{K cm}) \quad [22]$$

$$D = 7 \times 10^{-5}\,(\text{cm}^2/\text{s}) \quad [23\text{–}25]$$

$$k = 0.56 \quad [23\text{–}25]$$

$$m_\alpha = -2.6\,(\text{K/wt\%}) \quad [5, 26]$$

$$m_\beta = 2.4\,(\text{K/wt\%}) \quad [27]$$

Acknowledgement

This project was supported by Erciyes University Research Foundation. Authors would like to thank to Erciyes University Research Foundation for their financial support.

References

1. J. D. VERHEOVEN, "The Fundamentals of Physical Metallurgy," (John Wiley & Sons, Canada, 1975) p. 3.
2. S. N. TEWARI and R. SHAH, *Met. Trans.* **27A** (1996) 1353.
3. *Idem., ibid.* **23A** (1992) 3383.
4. J. T. MASON, J. D. VERHEOVEN and R. TRIVEDI, *J. Cryst. Growth.* **59** (1982) 516.
5. M. A. CHOPRA and S. N. TEWARI, *Met. Trans.* **22A** (1991) 2467.
6. C. M. KLAREN, J. D. VERHEOVEN and R. TRIVEDI, *ibid.* **11A** (1980) 1853.
7. E. ÇADIRLI, N. MARAŞLI, B. BAYENDER and M. GÜNDÜZ, *J. Mat. Sci.* **34** (1999) 5533.
8. F. YILMAZ and R. ELLIOT, *ibid.* **24** (1989) 2065.
9. M. GÜNDÜZ, Ph.D. thesis, Oxford University, 1984, p. 60.
10. D. G. MC CARTNEY, Ph.D. thesis, Oxford University, 1981, p. 96.
11. E. ÇADIRLI and M. GÜNDÜZ, *J. Mat. Process. Tech.* **97**(1–3) (1999) 73.
12. M. S. BHAT, D. R. POIRIER and J. C. HEINRICH, *Met. Trans.* **26B** (1995) 1049.
13. S. GANESAN, C. L. CHAN and D. R. POIRIER, *Mat. Sci. Eng.* **A151** (1992) 97.
14. J. D. HUNT, "solidification and Casting of Metals," (The Metal Society, London, 1979) p. 3.
15. W. KURZ and D. J. FISHER, *Acta Metall.* **29** (1981) 11.
16. S. A. MOIR and H. JONES, *Materials Letters* **12** (1991) 142.
17. C. T. RIOS and R. CARAM, *J. Cryst. Growth.* **174** (1997) 65.
18. R. TRIVEDI, *Met. Trans.* **15A** (1984) 977.
19. P. N. QUESTED and M. MCLEAN, *Mat. Sci. Eng.* **65** (1984) 171.
20. H. K. KIM, J. C. EARTHMAN and E. J. LAVERNIA, *ibid.* **A152** (1992) 240.
21. P. BARTOLOTTA, J. BARRETT, T. KELLY and R. SMASLEY, *JOM* **49** (5) (1997) 48.
22. M. GÜNDÜZ and J. D. HUNT, *Acta Metall.* **33**(9) (1985) 1651.
23. S. DE CHEVEIGNE, C. GUTHMANN and P. KUROWSKI, *J. Cryst. Growth.* **92** (1988) 616.
24. D. BOUCHARD and J. S. KIRKALDY, *Met. Trans.* **28B** (1997) 651.
25. W. A. TILLER and J. W. RUTTER, *Can. J. Physics* **34** (1956) 96.
26. S. N. TEWARI and M. A. CHOPRA, *J. Cryst. Growth.* **118** (1992) 183.
27. P. MAGNIN and R. TRIVEDI, *Acta Metall.* **39**(4) (1991) 453.

Received 14 June 1999
and accepted 3 February 2000